THE ASTROPHYSICAL JOURNAL, 636:L73–L76, 2006 January 10
© 2006. The American Astronomical Society. All rights reserved. Printed in U.S.A.

CONFIRMATION OF THE $E_{\rm peak}^{\rm src}$-$E_{\rm iso}$ (AMATI) RELATION FROM THE X-RAY FLASH XRF 050416A OBSERVED BY THE *SWIFT* BURST ALERT TELESCOPE

T. SAKAMOTO,[1,2] L. BARBIER,[1] S. D. BARTHELMY,[1] J. R. CUMMINGS,[1,2] E. E. FENIMORE,[3] N. GEHRELS,[1] D. HULLINGER,[4] H. A. KRIMM,[1,5] C. B. MARKWARDT,[1,4] D. M. PALMER,[3] A. M. PARSONS,[1] G. SATO,[6] AND J. TUELLER[1]

Received 2005 September 26; accepted 2005 December 6; published 2006 January 3

ABSTRACT

We report *Swift* Burst Alert Telescope (BAT) observations of the X-ray flash (XRF) XRF 050416A. The fluence ratio between the 15–25 and 25–50 keV energy bands of this event is 1.1, thus making it the softest gamma-ray burst (GRB) observed by BAT so far. The spectrum is well fitted by a Band function with $E_{\rm peak}^{\rm obs}$ of $15.0^{+2.3}_{-2.7}$ keV. Assuming the redshift of the host galaxy ($z = 0.6535$), the isotropic equivalent radiated energy $E_{\rm iso}$ and the peak energy at the GRB rest frame ($E_{\rm peak}^{\rm src}$) of XRF 050416A are not only consistent with the correlation found by Amati et al. and extended to XRFs by Sakamoto et al. but also fill in the gap of this relation around the 30–80 keV range of $E_{\rm peak}^{\rm src}$. This result tightens the validity of the $E_{\rm peak}^{\rm src}$-$E_{\rm iso}$ relation from XRFs to GRBs. We also find that the jet break time estimated using the empirical relation between $E_{\rm peak}^{\rm src}$ and the collimation corrected energy E_γ is inconsistent with the afterglow observation by the *Swift* X-Ray Telescope. This could be due to the extra external shock emission overlaid around the jet break time or to the nonexistence of a jet break feature for XRFs, which might be a further challenge for GRB jet emission models and XRF/GRB unification scenarios.

Subject heading: gamma rays: bursts

Online material: color figure

1. INTRODUCTION

Observations of X-ray flashes (XRF) are providing important information for understanding the nature of gamma-ray bursts (GRBs). Detailed studies of XRFs started a few years ago based on *BeppoSAX* observations (Heise et al. 2001; Kippen et al. 2003), but X-ray–rich events had already been detected by the *Ginga* satellite. Yoshida et al. (1989) reported that soft X-ray emission below 10 keV coexists with γ-ray emission of GRBs. About 36% of the bright bursts observed by *Ginga* have a value of $E_{\rm peak}^{\rm obs}$, the photon energy at which the νF_ν spectrum peaks, of around a few keV and also show large X-ray to γ-ray fluence ratios (Strohmayer et al. 1998).

The Wide-Field Camera (WFC) on board the *BeppoSAX* satellite observed 17 XRFs in 5 years (Heise et al. 2001). Kippen et al. (2003) searched for GRBs and XRFs that were observed in both WFC and BATSE. The WFC and BATSE joint spectral analysis of XRFs shows that their $E_{\rm peak}^{\rm obs}$ energies are significantly lower than those of the BATSE $E_{\rm peak}^{\rm obs}$ distribution (Preece et al. 2000). The systematic study of the spectral properties of XRFs observed by *HETE-2* also supports this result (Sakamoto et al. 2005a).

The afterglow detection and the redshift measurement from the host galaxy of XRF 020903, which is one of the softest XRFs observed by *HETE-2*, shows the dramatic progress in understanding the nature of XRFs. The prompt emission of XRF 020903 has $E_{\rm peak}^{\rm obs} < 5.0$ keV, which is 2 orders of magnitude smaller than that of typical GRBs. The optical transient and the host galaxy of XRF 020903 were detected. Further spectroscopic observation of the host galaxy suggests that the redshift is 0.25 ± 0.01 (Soderberg et al. 2004). Sakamoto et al. (2004) calculated the isotropic equivalent energy $E_{\rm iso}$ and the peak energy at the source frame $E_{\rm peak}^{\rm src}$ using the redshift of the host galaxy and found that XRF 020903 follows an extension of the empirical relationship between $E_{\rm iso}$ and $E_{\rm peak}^{\rm src}$ found by Amati et al. (2002) for GRBs (also known as the Amati relation). This result provides observational evidence that XRFs and GRBs form a continuum and are a single phenomenon.

In this paper, we report on the prompt emission properties of XRF 050416A as observed by the Burst Alert Telescope (BAT) on board the *Swift* satellite. The X-ray flash, XRF 050416A, was detected and localized by the *Swift* (Gehrels et al. 2004) BAT (Barthelmy et al. 2006) at 11:04:44.5 UTC on 2005 April 16 (Sakamoto et al. 2005b, 2005c). *Swift* autonomously slewed to the BAT on-board position, and both the *Swift* X-Ray Telescope (XRT; Burrows et al. 2006) and the UV-Optical Telescope (UVOT; Roming et al. 2006) detected the afterglow (G. Cusumano et al. 2006 and S. Holland et al. 2006, both in preparation). The afterglow emission of XRF 050416A was also observed by ground observatories at various wavelengths (Cenko et al. 2005a, 2005b; Anderson et al. 2005; Li et al. 2005; Kahharov et al. 2005; Price et al. 2005; Soderberg et al. 2005). Cenko et al. (2005c) reported that the host galaxy is faint and blue with a large amount of the star formation and that its redshift is $z = 0.6535 \pm 0.0002$. Throughout this paper, the quoted errors are at the 90% confidence level and the sky coordinates are in J2000.0 unless we state otherwise.

2. BAT DATA ANALYSIS

The BAT data analysis was performed using the *Swift* software package (HEAsoft 6.0). The background was subtracted using the modulations of the coded aperture (mask-weighting technique). In this technique, photons with energies higher than 150 keV become transparent to the coded mask and these photons are treated as a background. Thus, in this mask-weighted technique the effective BAT energy range is from 14 to 150 keV.

[1] NASA Goddard Space Flight Center, Code 661, Greenbelt, MD 20771.
[2] National Research Council, 2101 Constitution Avenue, NW, TJ2114, Washington, DC 20418.
[3] Los Alamos National Laboratory, P.O. Box 1663, Los Alamos, NM 87545.
[4] Department of Physics, University of Maryland, College Park, MD 20742.
[5] Universities Space Research Association, 10211 Wincopin Circle, Suite 500, Columbia, MD 21044-3432.
[6] Institute of Space and Astronautical Science, JAXA, Kanagawa 229-8510, Japan.

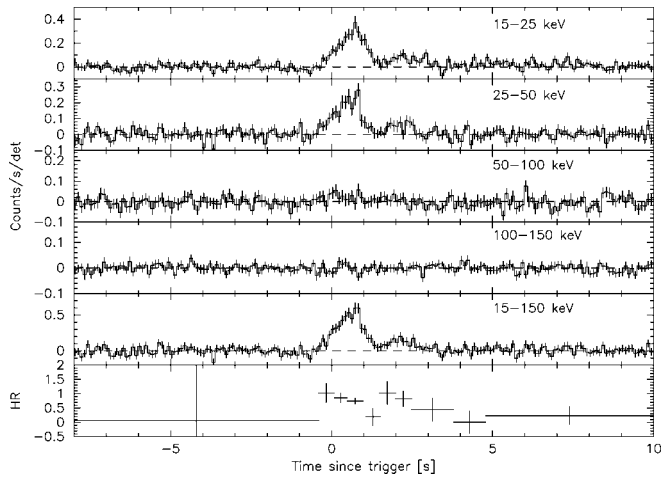

FIG. 1.—Light curve of XRF 050416A in five energy bands: 15–25, 25–50, 50–100, 100–150, and 15–150 keV. The bottom panel shows the hardness ratio between the 25–50 and 15–25 keV bands.

Figure 1 shows the energy-resolved BAT light curves of XRF 050416A. It is clear that the signal of the burst is only visible below 50 keV. The burst signal is composed of two peaks. The first peak has a triangular shape with the rise time longer than the decay time. When we calculate the spectral lag (Norris et al. 2000) between the 25–50 and 15–25 keV bands, the cross-correlation function lag is $-0.066^{+0.014}_{-0.018}$ s (1 σ error). These temporal characteristics are very unusual for typical GRBs (e.g., Mitrofanov et al. 1996; Norris et al. 2000); thus, it is difficult to understand them in the framework of the standard internal shock models in which the rise time is always shorter than the decay time and the hard emission always exceeds the soft emission (e.g., Piran 1999; Kobayashi et al. 1997). The t_{90} and t_{50} in the 15–150 keV band are 2.4 and 0.8 s, respectively. This t_{90} belongs to the shortest part of the "long GRB" classification based on the BATSE duration distribution (Paciesas et al. 1999). The fluence ratio between the 15–25 and the 25–50 keV bands of 1.1 makes this burst one of the softest GRBs observed by BAT so far. The bottom panel of Figure 1 shows the count ratio between the 25–50 and 15–25 keV bands. The spectral softening is clearly visible during the first and the second peak.

As reported by the BAT team,[7] we applied the energy dependent systematic error vector in the spectral files before doing any fitting procedure. The background-subtracted (mask-weighted) spectral data were used in the analysis. The XSPEC version 11.3.1 software package was used for fitting the data from 14 to 150 keV to the model spectrum.

Table 1 shows the fluences and the peak photon fluxes in the various energy bands. These fluences and peak photon fluxes were derived directly from fitting the time-averaged and 1 s peak spectra, respectively, assuming a Band function with $\alpha = -1$. Table 2 summarizes the spectral parameters of the BAT time-averaged spectrum.[8] Figure 2 shows the time-averaged spectrum, accumulated over the time interval from -0.5 to 3 s since the BAT trigger time, fitted with a simple power-law model. The photon index β, which is much steeper than -2, strongly indicates that the BAT observed the higher energy part of the Band function (Band et al. 1993). Motivated by this result, and also by the fact that almost all GRB and XRF spectra are well described by the Band function (Preece et al. 2000; Kippen et al. 2003), we tried to fit the spectrum with a Band function assuming the low-energy photon index α to be fixed at -1, which is the typical value for both GRBs (Preece et al. 2000) and XRFs (Kippen et al. 2003; Sakamoto et al. 2005a). The fitting shows a significant improvement from a simple power-law model to the Band function of $\Delta\chi^2 = 7.75$ for 1 degree of freedom. To quantify the significance of this improvement, we performed 10,000 spectral simulations assuming our best-fit spectral parameters in a simple power-law model and determined in how many cases the Band function fit gives χ^2 improvements of equal or greater than 7.75 over the simple power-law model. We found equal or higher improvements in χ^2 in 62 simulated spectra out of 10,000. Thus, the chance probability of having an equal or higher $\Delta\chi^2$ of 7.75 with the Band function when the parent distribution is a case of a simple power-law model is 0.6%. The observed $E_{\rm peak}$ energy, $E^{\rm obs}_{\rm peak}$, is well constrained at $15.6^{+2.3}_{-2.7}$ keV, and it confirms the soft nature of this burst. We also applied a *constrained* Band function fit (Sakamoto et al. 2004) to the BAT

[7] See http://legacy.gsfc.nasa.gov/docs/swift/analysis/bat_digest.html.

TABLE 1
ENERGY FLUENCES AND PEAK PHOTON FLUXES OF XRF 050416A ASSUMING A BAND FUNCTION WITH $\alpha = -1$

Energy Band (keV)	Energy Fluence (ergs cm^{-2})	Peak Photon Flux (photons cm^{-2} s^{-1})
15–25	$(1.7 \pm 0.2) \times 10^{-7}$	$2.9^{+0.4}_{-0.3}$
25–50	$(1.5 \pm 0.2) \times 10^{-7}$	1.7 ± 0.2
50–100	$3.4^{+1.0}_{-0.6} \times 10^{-8}$	$3.2^{+0.8}_{-0.4} \times 10^{-1}$
100–150	$4.2^{+11.8}_{-3.2} \times 10^{-9}$	$2.5^{+3.6}_{-1.2} \times 10^{-2}$
15–150	$(3.5 \pm 0.3) \times 10^{-7}$	5.0 ± 0.5

TABLE 2
THE TIME-AVERAGED SPECTRAL PARAMETERS OF XRF 050416A

Model	α	β	$E_{\rm peak}$	K_{30}	χ^2/dof
PL	...	-3.1 ± 0.2	...	$(4.3 \pm 0.3) \times 10^{-2}$	50.74/57
PL[a]	...	-3.4 ± 0.4	...	$(4.7 \pm 0.5) \times 10^{-2}$	43.88/53
Band	-1[b]	<-3.4	$15.6^{+2.3}_{-2.7}$	$3.5^{+1.7}_{-0.8} \times 10^{-1}$	42.99/56

NOTE.—$E_{\rm peak}$ is in units of keV; K_{30} is in units of photons cm^{-2} s^{-1} keV^{-1}.
[a] Fitting result using only spectral bins above 20 keV.
[b] Fixed.

[8] The spectral models that we use throughout this paper are a simple power-law model (PL), $f(E) = K_{30}(E/30)^{\beta}$, and the Band function, $f(E) = K_{30}(E/30)^{\alpha} \times \exp[-E(2+\alpha)/E_{\rm peak}]$ if $E < (\alpha-\beta)E_{\rm peak}/(2+\alpha)$ and $f(E) = K_{30}\{(\alpha-\beta) \times E_{\rm peak}/[30(2+\alpha)]\}^{\alpha-\beta} \exp(\beta-\alpha)(E/30)^{\beta}$ if $E \geq (\alpha-\beta)E_{\rm peak}/(2+\alpha)$.

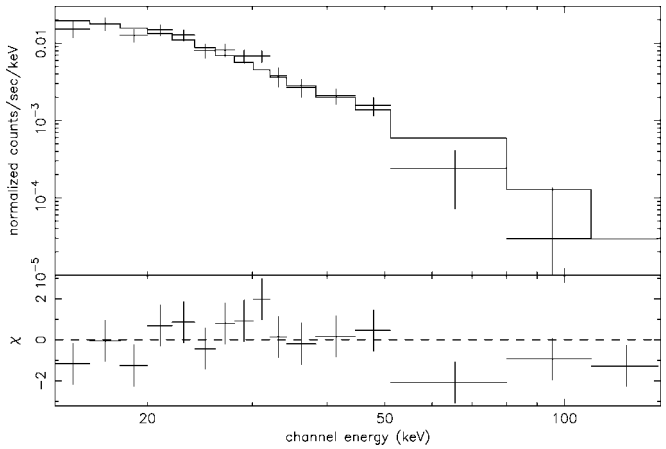

FIG. 2.—BAT spectrum of XRF 050416A with a simple power-law model. The spectral bins in the figure are at least 3 σ or are grouped into sets of 13 bins.

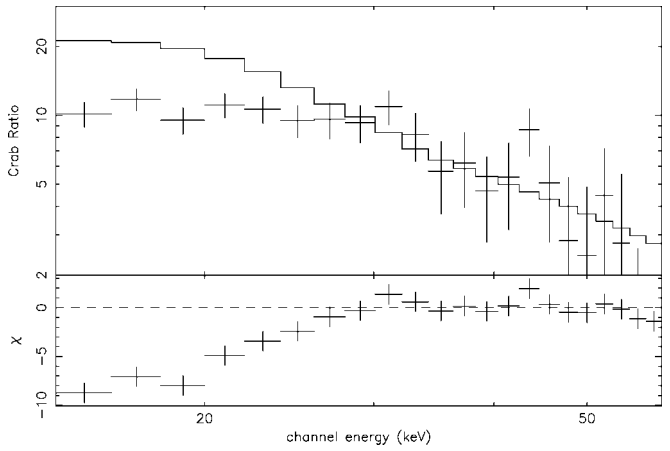

FIG. 3.—Ratio between the spectral data of XRF 050416A and the Crab Nebula. The numerator and denominator of the ratio are XRF 050416A and the Crab Nebula spectrum, respectively. The solid line shows the best-fit power-law slope of −1.9 derived from fitting the data above 25 keV. The bottom panel shows the residuals from this best-fit power-law slope. The reduced χ^2 is 7.72 for 20 degrees of freedom.

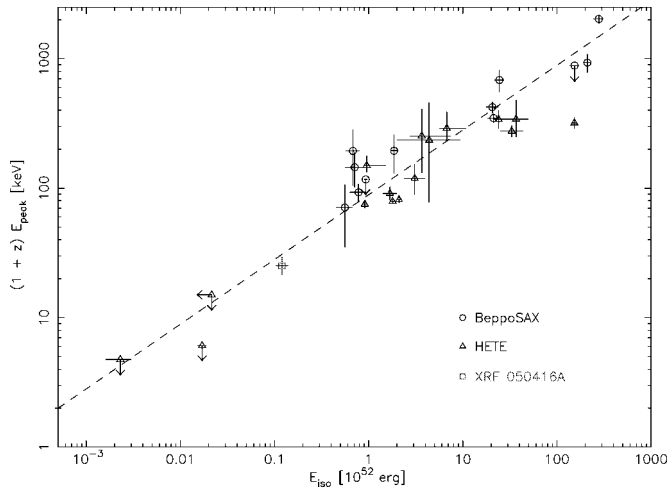

FIG. 4.—Isotropic equivalent energy, $E_{\rm iso}$, vs. the peak energy at the GRB rest frame, $E^{\rm src}_{\rm peak}$, for XRF 050416A (*square*) and the known redshift GRBs from *BeppoSAX* (*circles*) and *HETE-2* (*triangles*). The *BeppoSAX* GRB sample is from Amati et al. (2002), and the *HETE-2* GRB sample is from Lamb et al (2004). The dotted line is the relation $E^{\rm src}_{\rm peak} = 89(E_{\rm iso}/10^{52}\ {\rm ergs})^{0.5}$ (Amati et al. 2002). [*See the electronic edition of the Journal for a color version of this figure.*]

spectrum to estimate $E^{\rm obs}_{\rm peak}$. The calculated $E^{\rm obs}_{\rm peak}$ is consistent with a Band function fit of the fixed α to -1: 9.9 keV $< E^{\rm obs}_{\rm peak} <$ 20.0 keV at the 68% confidence level, 5.1 keV $< E^{\rm obs}_{\rm peak} <$ 21.8 keV at the 90% confidence level, and $E^{\rm obs}_{\rm peak} <$ 23.0 keV at the 99% confidence level.

The low-energy response is crucial for the determination of the spectral parameters of an XRF, and also, as reported by the BAT team,[9] there is a known problem of ∼15% smaller effective area in the Crab spectrum below 20 keV when fitting with a prelaunch response matrix. Since the postlaunch response matrix that we used in the analysis was applying a correction to force the Crab spectrum to fit a canonical model from 14 to 150 keV, and since we were also applying the systematic error vectors before performing the spectral analysis, the systematic effect of this low-energy problem is very limited. However, we investigated the spectrum of XRF 050416A ignoring the spectral bins below 20 keV. Even without using spectral bins below 20 keV, the photon index of XRF 050416A is -3.4 ± 0.4, much steeper than -2 ($\alpha < -2$ at the >99.99% confidence level). Furthermore, we took the ratio of the spectral data of XRF 050416A and the Crab Nebula observed at an incident angle similar to that of XRF 050416A. The result is shown in Figure 3. The flattening trend of the photon index below 25 keV is also clear in this figure. Thus, we conclude that the deviation from a simple power-law model below 25 keV is a real feature of the spectrum of XRF 050416A.

3. DISCUSSION

One of the most important discoveries related to XRF 050416A is the confirmation of the $E^{\rm src}_{\rm peak}$-$E_{\rm iso}$ relation (Amati et al. 2002). We calculate the $E_{\rm peak}$ energy at the GRB rest frame, $E^{\rm src}_{\rm peak}$, and the isotropic equivalent energy (1–10^4 keV at the rest frame), $E_{\rm iso}$, using the redshift of the host galaxy ($z = 0.6535$). Assuming $\alpha = -1$, the $E^{\rm src}_{\rm peak}$ and $E_{\rm iso}$ values of XRF 050416A are $25.1^{+4.4}_{-3.7}$ keV and $(1.2 \pm 0.2) \times 10^{51}$ ergs, respectively. Figure 4 shows the data point of XRF 050416A with the known redshift GRBs of *BeppoSAX* and *HETE-2* samples (Amati 2003; Lamb et al. 2004; Sakamoto et al. 2004). XRF 050416A not only follows the $E^{\rm src}_{\rm peak} \propto E^{0.5}_{\rm iso}$ relation but also fills in the gap of the relation around $E^{\rm src}_{\rm peak} =$ 30–80 keV. This result tightens the validity of this relation by 5 orders of magnitude in $E_{\rm iso}$ and 3 orders of magnitude in $E^{\rm src}_{\rm peak}$. XRF 050416A bridges the gap in the $E^{\rm src}_{\rm peak}$-$E_{\rm iso}$ relation between XRFs, which have $E^{\rm src}_{\rm peak}$ of less than 10 keV, and GRBs.

The confirmation of the $E^{\rm src}_{\rm peak}$-$E_{\rm iso}$ relation from XRFs to GRBs gives us a clear indication that XRFs and GRBs form a continuum and are a single phenomenon. There are several jet models to explain a unified picture of XRFs and GRBs. The off-axis jet model (Yamazaki et al. 2004; Toma et al. 2005), the structured jet model (Rossi et al. 2002; Zhang & Mészáros 2002; Zhang et al. 2004), and the variable jet opening angle model (Lamb et al. 2005) are the most popular models in this aspect. On the other hand, there are theoretical models to explain XRFs in the framework of the internal shock model (Mészáros et al. 2002; Mochkovitch et al. 2004) and of the external shock model (Dermer et al. 1999; Huang et al. 2002; Dermer & Mitman 2004). The cited jet models and internal/external shock models not only explain the existence of XRFs under certain assumptions, but also, in some of their realizations or for some values of their parameters, they can predict the $E^{\rm src}_{\rm peak}$-$E_{\rm iso}$ correlation.

According to the XRT afterglow observations of XRF 050416A, the decay slope of the afterglow emission is ~ -0.9 from 0.015 to ∼34.7 days after the GRB trigger without any signature of a jet break (G. Cusumano et al. 2006, in preparation; Nousek et al. 2005).

Using $E^{\rm src}_{\rm peak}$ and $E_{\rm iso}$ of XRF 050416A measured by BAT, we can estimate the jet break time using the relation between $E^{\rm src}_{\rm peak}$ and the jet collimation corrected energy E_γ found by Ghirlanda et al. (2004; the Ghirlanda relation). However, there is a debate about the assumption of the jet model used by Ghirlanda et al. (2004) to derive the relationship between $E^{\rm src}_{\rm peak}$ and E_γ (Xu 2005; Liang & Zhang 2005). Based on this argument, we use the empirical relation between $E_{\rm iso}$, $E^{\rm src}_{\rm peak}$, and the jet break time at the rest frame, $t^{\rm src}_{\rm jet}$, derived by Liang & Zhang (2005). Note that there is no assumption of a jet model in the formula found by Liang & Zhang (2005), and thus their relation

[9] See the "Corrections to Response" section of the BAT Digest (http://legacy.gsfc.nasa.gov/docs/swift/analysis/bat_digest.html).

is purely based on observational properties. When we use equation (5) of Liang & Zhang (2005), $E_{\rm iso}/10^{52}$ ergs $= 0.85 \times (E^{\rm src}_{\rm peak}/100\ {\rm keV})^{1.94}(t^{\rm src}_{\rm jet}/1\ {\rm day})^{-1.24}$, the jet break time in the observer's frame is estimated to be ~1.5 days after the GRB onset time. Note that this estimated jet break time is consistent with the estimation using the Ghirlanda relation assuming a circumburst density of 3 cm^{-3}. Thus, the estimated jet break time using the empirical $E^{\rm src}_{\rm peak}$-$E_{\rm iso}$-$t^{\rm src}_{\rm jet}$ relation is inconsistent with the null detection of a jet break until more than 34.3 days after the trigger by XRT.

In the off-axis jet model (Yamazaki et al. 2004; Toma et al. 2005), the null detection of the jet break in the XRT data of XRF 050416A could be difficult to explain. When we assume a bulk Lorentz factor of 100, $E^{\rm src}_{\rm peak}$ of 300 keV for an on-axis observer, and a jet opening angle of 2°, the viewing angle from the jet on-axis is estimated to be ~4° from the observed $E^{\rm src}_{\rm peak}$ of 25 keV. According to Granot et al. (2002), when observing the jet from an angle 2 times larger than the jet opening angle, we would expect to see a rise in the flux around 1 day after the burst. It is possible to increase the bulk Lorentz factor and to reduce the off-axis viewing angle to achieve the same Doppler factor. However, in this case, the afterglow light curve should be close to the on-axis case; thus, we would expect to see a jet break around the time we estimated.

On the other hand, the variable jet opening angle model (Lamb et al. 2005) might work for XRF 050416A if E_γ is a constant value. If we assume the values typical for GRBs ($E^{\rm src}_{\rm peak} = 300$ keV and a jet opening angle of 5°), the jet opening angle of XRF 050416A is calculated to be 52° because of the inverse relation between $E^{\rm src}_{\rm peak}$ and the jet opening angle in the case in which E_γ is a constant. When we use the formulation of Sari et al. (1999) applying the estimated jet opening angle, the jet break time is 64 days in the case of a circumburst density of 10 cm^{-3}. Both the low $E^{\rm src}_{\rm peak}$ and the null detection of the jet break could be explained in the variable jet opening angle model if E_γ is constant. However, as Ghirlanda et al. (2004) showed, E_γ is not a constant parameter but has a good correlation with $E^{\rm src}_{\rm peak}$. When we apply the Ghirlanda relation, $E^{\rm src}_{\rm peak} \propto E_\gamma^{0.7}$, in the variable opening angle model and recalculate the jet break time, the break time is 0.7 days assuming a circumburst density of 10 cm^{-3}. In the variable jet opening angle model, there is no way to explain both the Ghirlanda relation and the null detection of the jet break by XRT simultaneously.

One natural way to explain the nondetection of the jet break feature is that extra components are overlaid around a jet break time period. According to the afterglow calculations in the X-ray band by Zhang et al. (2006), there are several possibilities for hiding a jet break feature due to some kind of emission by the external shock. These are external shock emission from (1) the dense clouds surrounding a GRB progenitor (e.g., Lazzati et al. 2002), (2) a moderately relativistic cocoon component of a two-component jet (e.g., Granot 2005), and (3) a jet with large fluctuations in angular direction (patchy jets; Kumar & Piran 2000). On the other hand, it might be the case that XRFs indeed do not show the signature of a jet break in the afterglow. Indeed, although the numbers in the sample are limited, there is no clear observational indication of a jet break in any XRF afterglow light curve so far. If the later case is true, we need to change our view of XRFs completely. Thus, the multiwavelength observations of XRF afterglows will be crucial to investigate whether a jet break feature exists in XRFs or not.

We would like to thank R. Yamazaki and D. Q. Lamb for useful comments and discussions. We would also like to thank the anonymous referee for comments and suggestions that materially improved the paper. This research was performed while T. S. held a National Research Council Research Associateship at NASA Goddard Space Flight Center.

REFERENCES

Amati, L. 2003, Chinese J. Astron. Astrophys., 3 (Suppl.), 455
Amati, L., et al. 2002, A&A, 390, 81
Anderson, G., et al. 2005, GCN Circ. 3266, http://gcn.gsfc.nasa.gov/gcn/gcn3/3266.gcn3
Band, D. L., et al. 1993, ApJ, 413, 281
Barthelmy, S. D., et al. 2006, Space Sci. Rev., in press
Burrows, D., et al. 2006, Space Sci. Rev., in press
Cenko, S. B., et al. 2005a, GCN Circ. 3265, http://gcn.gsfc.nasa.gov/gcn/gcn3/3265.gcn3
———. 2005b, GCN Circ. 3269, http://gcn.gsfc.nasa.gov/gcn/gcn3/3269.gcn3
———. 2005c, GCN Circ. 3542, http://gcn.gsfc.nasa.gov/gcn/gcn3/3542.gcn3
Dermer, C. D., Chiang, J., & Böttcher, M. 1999, ApJ, 513, 656
Dermer, C. D., & Mitman, K. E. 2004, in ASP Conf. Ser. 312, Third Rome Workshop on Gamma-Ray Bursts in the Afterglow Era, ed. M. Feroci et al. (San Francisco: ASP), 301
Gehrels, N., et al. 2004, ApJ, 611, 1005
Ghirlanda, G., Ghisellini, G., & Lazzati, D. 2004, ApJ, 616, 331
Granot, J. 2005, ApJ, 631, 1022
Granot, J., Panaitescu, A., Kumar, P., & Woosley, S. E. 2002, ApJ, 570, L61
Heise, J., in 't Zand, J., Kippen, R. M., & Woods, P. M. 2001, in Gamma-Ray Bursts in the Afterglow Era, ed. E. Costa, F. Frontera, & J. Hjorth (Berlin: Springer), 16
Huang, Y. F., Dai, Z. G., & Lu, T. 2002, MNRAS, 332, 735
Kahharov, B., et al. 2005, GCN Circ. 3274, http://gcn.gsfc.nasa.gov/gcn/gcn3/3274.gcn3
Kippen, R. M., Woods, P. M., Heise, J., in 't Zand, J., Briggs, M. S., & Preece, R. D. 2003, in AIP Conf. Proc. 662, Gamma-Ray Burst and Afterglow Astronomy 2001, ed. G. R. Ricker & R. Vanderspek (Melville: AIP), 244
Kobayashi, S., Piran, T., & Sari, R. 1997, ApJ, 490, 92
Kumar, P., & Piran, T. 2000, ApJ, 532, 286
Lamb, D. Q., Donaghy, T. Q., & Graziani, C. 2005, ApJ, 620, 355
Lamb, D. Q., et al. 2004, NewA Rev., 48, 423
Lazzati, D., et al. 2002, A&A, 396, L5
Li, W., et al. 2005, GCN Circ. 3270, http://gcn.gsfc.nasa.gov/gcn/gcn3/3270.gcn3
Liang, E., & Zhang, B. 2005, ApJ, 633, 611
Mészáros, P., Ramirez-Ruiz, E., Rees, M. J., & Zhang, B. 2002, ApJ, 578, 812
Mitrofanov, I. G., et al. 1996, ApJ, 459, 570
Mochkovitch, R., Daigne, F., Barraud, C., & Atteia, J. L. 2004, in ASP Conf. Ser. 312, Third Rome Workshop on Gamma-Ray Bursts in the Afterglow Era, ed. M. Feroci et al. (San Francisco: ASP), 381
Norris, J. P., Marini, G. F., & Bonnel, J. T. 2000, ApJ, 534, 248
Nousek, J. A., et al. 2005, ApJ, submitted (astro-ph/0508332)
Paciesas, W. S., et al. 1999, ApJS, 122, 465
Piran, T. 1999, Phys. Rep., 314, 575
Preece, R. D., et al. 2000, ApJS, 126, 19
Price, P. A., et al. 2005, GCN Circ. 3312, http://gcn.gsfc.nasa.gov/gcn/gcn3/3312.gcn3
Roming, P., et al. 2006, Space Sci. Rev., in press
Rossi, E., Lazzati, D., & Rees, M. J. 2002, MNRAS, 332, 945
Sakamoto, T., et al. 2004, ApJ, 602, 875
———. 2005a, ApJ, 629, 311
———. 2005b, GCN Circ. 3264, http://gcn.gsfc.nasa.gov/gcn/gcn3/3264.gcn3
———. 2005c, GCN Circ. 3273, http://gcn.gsfc.nasa.gov/gcn/gcn3/3273.gcn3
Sari, R., Piran, T., & Halpern, J. P. 1999, ApJ, 519, L17
Soderberg, A. M., et al. 2004, ApJ, 606, 994
———. 2005, GCN Circ. 3318, http://gcn.gsfc.nasa.gov/gcn/gcn3/3318.gcn3
Strohmayer, T. E., Fenimore, E. E., Murakami, T., & Yoshida, A. 1998, ApJ, 500, 873
Toma, K., Yamazaki, R., & Nakamura, T. 2005, ApJ, 635, 481
Xu, D. 2005, ApJ, submitted (astro-ph/0504052)
Yamazaki, R., Ioka, K., & Nakamura, T. 2004, ApJ, 607, L103
Yoshida, A., et al. 1989, PASJ, 41, 509
Zhang, B., Dai, X., Lloyd-Ronning, N. M., & Mészáros, P. 2004, ApJ, 601, L119
Zhang, B., & Mészáros, P. 2002, ApJ, 571, 876
Zhang, B., et al. 2006, ApJ, in press (astro-ph/0508321)